Brownian dynamics of hard spherocylinders

Hartmut Löwen
Sektion Physik der Universität München, Theresienstrasse 37, D-80333 München, Germany
(Received 22 February 1994)

A model of hard spherocylinders exhibiting Brownian dynamics in a solvent is investigated by Brownian dynamics simulations. Long-time translational and rotational self-diffusion coefficients are calculated in the disordered phase over the whole range of densities and a ratio p of total length to width ranging from 1 to 6. A simple analytical formula is given to fit the results. The self-diffusion coefficients are also obtained along the fluid freezing line for arbitrary p. Measured in terms of their short-time limits, both self-diffusion coefficients are *nonmonotonic* in p. For $2 \leq p \leq 6$, the long-time to short-time rotational self-diffusion ratio is about 0.12, which constitutes a simple dynamical phase transition rule for the fluid-nematic and fluid-crystalline transition.

PACS number(s): 61.30.−v, 66.10.−x, 82.70.−y

I. INTRODUCTION

Diffusion processes in concentrated rigid-rod-like systems are dominated by entangling effects due to the repulsion of arbitrarily oriented vicinal rods which form effective cages. Both the mean-square displacement of the center-of-mass coordinate as well as the rotational degree of freedom exhibit diffusive behavior for long times whose details depend sensitively on the rod density, the temperature, and the rod interaction [1]. In order to get insight into the dynamical relaxation of rods, three different routes can be followed. First, *experimental* methods such as birefringence and forced-Rayleigh scattering or dynamical light scattering [2–8] can be applied to measure the long-time diffusive relaxation of the orientational and translational rod motion. Unfortunately the experiments are performed on rather complex supramolecular aggregates whose detailed dynamics and interactions, required as a necessary input for computer simulation and theory, are not known exactly. Typical experimental samples are solutions of rigid-rod-like polymers, ellipsoidal and cylindrical micelles, and suspensions of colloidal rods such as tobacco mosaic or *fd* viruses. Sometimes they suffer also from a high intrinsic polydispersity. Since all these samples are embedded in a solvent their dynamics is of Langevin rather than of Newtonian type. If the spatial dimension of the rods is mesoscopic, a complete time scale separation between solvent and rod relaxation justifies the picture of Brownian dynamics where the solvent exhibits random kicks on the rods.

Second, self-diffusion in some simple models of rigid rods was studied by Brownian dynamics *computer simulations.* The simplest model that was investigated is that of infinitely thin needles of length L and concentration ρ; see Doi, Yanamoto, and Kano [9]. The concentration dependence of the rotational diffusion constant is by now well understood even for very long needles. A different simple phenomenological model for the rod interaction was proposed and studied by Fixman [10] which was then further investigated by Brownian dynamics simulations [11].

Third, as regards theory, Doi and Edwards have proposed a tube model [12,13] predicting that the rotational long-time diffusion coefficient scales as $(\rho L^3)^{-2}$ for high concentration. This model was later refined by Teraoka, Ookubo, and Hayakawa [14]. Fixman [10] proposed a simple analytical formula for the rotational diffusion coefficient based on the rapid dissipation of cage forces. Using Brownian dynamics simulations [11] Fixman's prediction was confirmed for moderate but not for high concentrations. More recently, also a Green function formulation [15] as well as a dynamic mean-field theory [16] were applied to the needle model in order to predict long-time self-diffusion properties.

The simulations and the theoretical work mainly focuses on simple models which are, however, not very realistic to describe the rod interaction and dynamics. For *sterically-stabilized* index-matched suspensions is more realistic than the needle model. Also *charged-stabilized* rod-like suspensions with a high concentration of added salt [17] behave like bodies with finite excluded volume. In the low-salt-concentration regime, on the other hand, the interaction between charged-stabilized colloidal rods can be described in terms of a Yukawa segment model introduced by Klein and co-workers [18–20] which was recently confirmed by *ab initio* simulations [21].

In this paper, a systematic investigation of the hard-spherocylinder model with Brownian dynamics is presented. The motivation to study this model is threefold: First, for colloidal suspensions it is a more realistic model than those studied before. Second, it is still simple enough insofar as it is characterized by two parameters only, namely, the length to width ratio and the packing fraction of the rods. These parameters determine completely the bulk phase diagram which is known from Monte Carlo simulation [22] and theory [23,24]. Therefore the model could, in principle, be addressed also by theory. Third, in contrast to the needle model where very long rods are considered, we study moderate length to width ratios p up to $p=6$. In particular, the isotropic case is included and we study how anisotropies of the in-

teraction influence the long-time dynamics. From this aspect the results of this paper are complementary to the simulation of the needle model [9].

In our simulations, Brownian dynamics of the rods are characterized by a parallel, a perpendicular, and a rotational short-time diffusion constant. Hydrodynamic interactions are neglected. The long-time diffusion coefficients are then calculated by computer simulation over the whole range of packing fraction of the disordered (fluid) phase and a length to width ratio ranging from 1 (spheres) to 6. There are also molecular dynamics simulations for hard-rod-like systems which is an adequate dynamics for molecular liquid crystals (see, e.g., [25–27]) but not for liquids embedded in a solvent. It turns out that Brownian dynamics simulations are computationally more costly since the time step has to be very small in the simulation.

It is instructive to compare with Brownian dynamics of *spheres* where only the translational motion is nontrivial. In this case much more is known: Brownian dynamics simulations of hard spheres for arbitrary packing fraction in the fluid phase have been carried out by Cichocki and Hinsen [28,29]. Mode-coupling theories and Enskog-type approaches have successfully been applied to predict the long-time self-diffusion [30]. At freezing the ratio of the long-time and short-time self-diffusion coefficient D_L^t/D^t is 0.100. The latter value is universal since it is the same also for soft interaction which constitutes a *dynamical freezing rule* [31]. For spheres theories and extensive simulations have been done also for Yukawa potentials [32] and a detailed comparison with the experimental data was performed [33]. Even effects of polydispersity on self-diffusion have been studied [34,35].

It is tempting to look for a generalization of the dynamical phase transition rule for anisotropic liquids. We have calculated the translational and rotational long-time self-diffusion coefficients D_L^t and D_L^r along the fluid freezing line and measured them in terms of their short-time limits D^t and D^r. Here we have considered also higher length to width ratios p including the Onsager limit $p \to \infty$. Depending on p there are two possible coexisting phases, a crystal or a nematic. As a result, both D_L^t/D^t and D_L^r/D^r are nonmonotonic in p which rules out a general universal phase transition rule which is valid for any p. However, in a good approximation, D_L^r/D^r is roughly independent of p along the fluid freezing line for $2 \le p \le 6$ where it equals 0.12. This results in a simple dynamical phase transition rule for the isotropic-crystalline and isotropic-nematic transition in the restricted regime $2 \le p \le 6$.

The paper is organized as follows: In Sec. II, we discuss Brownian dynamics in our model of hard spherocylinders. Then we describe the simulational method in Sec. III. Results for the pair structure and the diffusion coefficients are then collected in Secs. IV and V. Finally we are also looking for dynamical empirical freezing criteria for anisotropic liquids in Sec. VI where we also include results for larger length to width ratios on the fluid-nematic coexistence line. Our calculations do not show a general universality of the dynamical quantities at the fluid freezing line, ruling out a simple general dynamical phase transition rule but establishing one in the restricted regime $2 \le p \le 6$. Finally Sec. VII is devoted to some conclusive comments.

II. MODEL

We consider N spherocylinders in a volume V with total width L and diameter σ; see Fig. 1. A rod configuration is characterized by its center-of-mass coordinates $\{\mathbf{R}_i,\ i=1,\ldots,N\}$ and orientations $\{\mathbf{\Omega}_i,\ i=1,\ldots,N\}$ where $\mathbf{\Omega}_i$ is a unit vector. The potential energy is simply of the excluded-volume type: It is zero if the rods do not overlap and infinite otherwise. Due to this simple interaction the temperature T scales out and the rod number density $\rho=N/V$ is the only thermodynamic variable. This density is conveniently expressed in terms of the rod packing fraction $\eta=\rho\pi\sigma^2[\sigma/6+(L-\sigma)/4]$. Choosing the rod diameter σ as the typical length scale, the only additional geometric quantity is the length to width ratio $p=L/\sigma$ of the rods. Hence all structural and thermodynamic quantities including the bulk phase diagram only depend on η and p. For $L=\sigma$ the isotropic case of hard spheres is recovered.

We adopt Brownian dynamics of the rods and approximate the short-time dynamics by that of one single rod in a solvent characterized by two translational short-time diffusion constants, $D^\perp$ and $D^\parallel$, perpendicular and parallel to the rod axis, and a rotational short-time diffusion constant D^r. As a function of p, these three diffusion constants have been calculated by Broersma [36] and Tirado and co-workers [37,38]. For the calculations in this paper we have used the analytical expression proposed by Tirado, Martinez, and de la Torre in Ref. [38]:

$$D^\perp=\frac{D_0}{4\pi}(\ln p+0.839+0.185/p+0.233/p^2)\,, \tag{1}$$

$$D^\parallel=\frac{D_0}{2\pi}(\ln p-0.207+0.980/p-0.133/p^2)\,, \tag{2}$$

$$D^r=\frac{3D_0}{\pi L^2}(\ln p-0.662+0.917/p-0.050/p^2)\,, \tag{3}$$

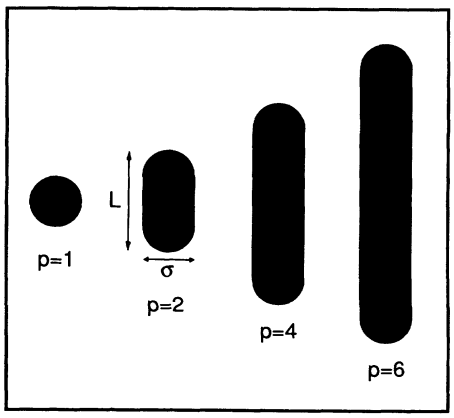

FIG. 1. Shape of the spherocylinders for different values of the length to width ratio $p=L/\sigma$. The cases $p=1,2,4,6$ which are used in the simulations are shown.

with

$$D_0 = k_B T/\eta_s L \ , \tag{4}$$

where k_B is Boltzmann's constant and η_s the shear viscosity of the solvent. These different diffusion coefficients are displayed as a function of p in Fig. 2.

Two remarks are in order: First, strictly speaking, Eqs. (1)–(3) are valid for a pure cylinder but not for a spherocylinder. We have, however, assumed that the diffusion constants of a pure cylinder and a spherocylinder of equal total length do not differ much. The differences are maximal for spheres ($p=1$) where one gets $D^{\perp}/D_0=0.100$ and $D^{\parallel}/D_0=0.102$ from Tirado, Martinez, and de la Torre's expression. Both values essentially do not differ much from the exact Stokes result $D^{\perp}/D_0=D^{\parallel}/D_0=1/3\pi=0.106\ldots$. Hence the differences between a pure cylinder and a spherocylinder are negligibly small. Furthermore, it was shown [38] that Eqs. (1)–(3) are compatible with experimental data in the range $2 \le p \le 30$, also proving that it is a reasonable fit for the diffusion constants.

The second point is more severe. In using the type of dynamics described above any hydrodynamic interactions from vicinal rods mediated by the solvent are neglected. These interactions do not influence the statics and the bulk phase diagram but they alter dynamical correlations. For high packing fractions they become relevant in slowing down the diffusive short-time as well as long-time relaxation. Unfortunately the explicit form of the hydrodynamic interactions is only known asymptotically for larger rod separations but not for intermediate and high rod concentrations. Consequently, at the moment, it is not clear how to incorporate them into the model. Nevertheless there are two points which strongly motivate an analysis of our model without hydrodynamic interactions.

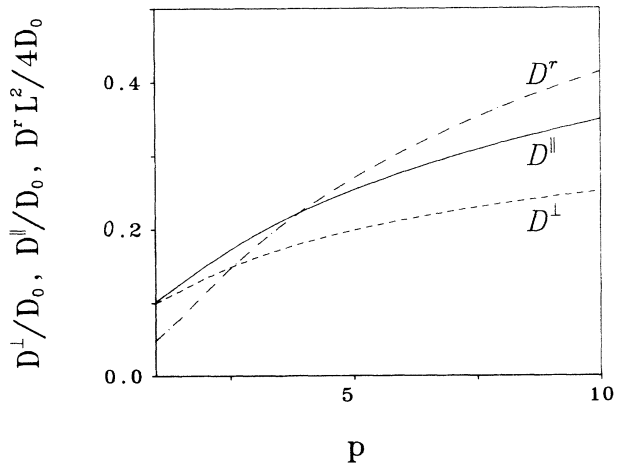

FIG. 2. Free- or short-time diffusion constants of a single cylinder in a solvent versus length to width ratio p, $1 \le p \le 10$. The parallel translational diffusion constant $D^{\parallel}$ is given by the solid line and the perpendicular translational diffusion constant $D^{\perp}$ by the dashed line. Both $D^{\parallel}$ and $D^{\perp}$ are given in units of D_0. The dot-dashed line is the rotational diffusion constant D^r which is given in units of $4D_0/L^2$.

(i) Often the hard-spherocylinder model with an effective diameter is employed to model the interaction of charge colloidal rods; see, e.g., [39]. This idea was first indicated by Onsager [40]. Then the true hydrodynamic diameter of the rods is much smaller than the effective diameter such that hydrodynamic interaction can safely be neglected. For this case the Brownian dynamics of the substitute hard-spherocylinder system has direct significance.

(ii) In discussing long-time diffusion coefficients of *spheres,* Medina-Noyola [41] proposed a simple scaling. He gives evidence for the fact that the ratio of long-time and short-time diffusion coefficients remains unaffected by hydrodynamic interactions. It is this ratio which we shall discuss in the following for rods. Hence there is reason to believe that this ratio is not significantly changed by hydrodynamic interactions.

In ordinary Brownian dynamics simulations, trajectories of the center-of-mass and orientational coordinates are generated by integrating the corresponding Langevin equations with a finite time step Δt. For spheres this was implemented by Ermak [42], for another calculation see also [43]. The corresponding finite difference equations for rods are a bit more complicated. At a given time t, the center-of-mass position $\mathbf{R}_i(t)$ of the ith rod can be split into a part $\mathbf{R}_i^{\parallel}(t) \equiv [\mathbf{\Omega}_i(t)\cdot\mathbf{R}_i(t)]\mathbf{\Omega}_i(t)$ parallel and another part $\mathbf{R}_i^{\perp}(t)$ perpendicular to the rod orientation $\mathbf{\Omega}_i(t)$ such that

$$\mathbf{R}_i(t)=\mathbf{R}_i^{\parallel}(t)+\mathbf{R}_i^{\perp}(t) \ . \tag{5}$$

The same separation into a parallel and perpendicular part can be done for the total force $\mathbf{F}_i(t)$, acting on the ith rod due to the interaction with the other rods,

$$\mathbf{F}_i(t)=\mathbf{F}_i^{\parallel}(t)+\mathbf{F}_i^{\perp}(t) \ . \tag{6}$$

Then for a finite time step Δt the temporal evolution of $\mathbf{R}_i(t)$ is given by

$$\mathbf{R}_i^{\parallel}(t+\Delta t)=\mathbf{R}_i^{\parallel}(t)+\frac{D^{\parallel}}{k_B T}\mathbf{F}_i^{\parallel}(t)\Delta t+(\Delta R^{\parallel})\mathbf{\Omega}_i(t) \ , \tag{7}$$

where $(\Delta R^{\parallel})$ is a random displacement due to solvent kicks which is a Gaussian distributed random number with zero mean, $(\Delta R^{\parallel})=0$, and variance

$$\overline{(\Delta R^{\parallel})^2}=2D^{\parallel}\Delta t \ . \tag{8}$$

Here, $\overline{(\ )}$ denotes an average over a Gaussian distribution.

The perpendicular part, on the other hand, diffuses with the perpendicular diffusion constant $D^{\perp}$:

$$\mathbf{R}_i^{\perp}(t+\Delta t)=\mathbf{R}_i^{\perp}(t)+\frac{D^{\perp}}{k_B T}\mathbf{F}_i^{\perp}(t)\Delta t +(\Delta R_1^{\perp})\mathbf{e}_{i1}(t)+(\Delta R_2^{\perp})\mathbf{e}_{i2}(t) \ , \tag{9}$$

where again $(\Delta R_1^{\perp})$ and $(\Delta R_2^{\perp})$ are Gaussian distributed with zero mean and variance $2D^{\perp}\Delta t$. Furthermore, $\mathbf{e}_{i1}(t)$ and $\mathbf{e}_{i2}(t)$ are two orthogonal unit vectors perpendicular to $\mathbf{\Omega}_i(t)$.

Finally the orientational degree of freedom diffuses as

$$\mathbf{\Omega}_i(t+\Delta t)=\mathbf{\Omega}_i(t)+\frac{D^r}{k_BT}\mathbf{M}_i(t)\times\mathbf{\Omega}_i(t)\Delta t + x_1\mathbf{e}_{i1}(t)+x_2\mathbf{e}_{i2}(t)\ , \quad (10)$$

where now $\mathbf{M}_i(t)$ is the torque acting on rod i and x_1, x_2 are Gaussian random numbers with zero mean and variance $2D^r\Delta t$.

If the time step Δt is very small, the leading terms in Eqs. (7), (9), and (10) are the random displacements. The square root of the diffusion constants $D^{\parallel}/D_0$ and $D^{\perp}/D_0$ which are shown in Fig. 2 is proportional to the mean displacements parallel and perpendicular to the director. The square root of $D^rL^2/4D_0$, on the other hand, is proportional to the mean random displacement due to orientational short-time diffusion for a point on the top of the rod having a distance of $L/2$ from the center-of-mass coordinate. Figure 2 shows that this displacement exceeds the translational displacements for large p whereas for small p the translational displacement becomes larger.

III. SIMULATION TECHNIQUE

Equations (7)–(10) constitute the basis for Brownian dynamics simulations of rods: For a given rod configuration and a given time t all forces $\{\mathbf{F}_i(t)\}$ and torques $\{\mathbf{M}_i(t)\}$ are calculated according to the rod interaction and then the rods are moved in parallel to get a new configuration by adding a random displacement. This results in "toothed" trajectories $\{\mathbf{R}_i(t)\},\{\mathbf{\Omega}_i(t)\}$ $(i=1,\ldots,N)$ for which dynamical correlation can be extracted. For hard-body interactions, however, this scheme cannot directly be used since the forces and torques are either zero or infinite. Hence one has to avoid and exclude overlapping rod configurations. Also it is numerically more efficient to use a scheme where the rods are moved sequentially instead of in parallel. This results in the following algorithm: We choose a small time step Δt. In one elementary trial step of the simulation, one out of N rods is randomly chosen. In the first part of an elementary trial step, the translational degrees of freedom are then moved with zero force according to Eqs. (7) and (9). If this results in a nonoverlapping configuration, the move is accepted which means that the center-of-mass coordinate of the chosen particle is updated. In the opposite case of a rod overlap the move is rejected and the center-of-mass coordinates are not changed. Then in the second part of an elementary trial step, the orientational degree of freedom is moved with zero torque according to Eq. (10). Again, only moves are accepted that do not lead to an overlap with vicinal rods. For the sake of completeness, the overlap conditions of two rods are listed in Appendix A.

This algorithm is basically a Monte Carlo scheme. Structural quantities and static correlations are independent of Δt. Therefore, if one is only interested in static correlations, one can optimize Δt by maximizing the acceptance-rejection ratio. For hard spherocylinders, such Monte Carlo simulations have been widely used for almost 20 years, see [44]. The important point for our use is that this sequential algorithm is stochastically equivalent to Brownian dynamics of rods in the limit $\Delta t \searrow 0$ if the corresponding time t associated to N_e elementary trial steps is taken as [28]

$$t=N_e\Delta t/N\ . \quad (11)$$

Hence, in contrast to the static correlations, the dynamical correlations do depend on Δt. Consequently, Δt has to be chosen sufficiently small, which implies that a huge number of elementary trial steps (typically 2×10^8) are needed in order to get correct statistical averages for long-time properties.

In our calculations, a cubic simulational box containing N rods with periodic boundary conditions is used. The ratio p of total length and width is changed between 1 and 6. For $p=1$ (spheres), the orientational motion never leads to an overlapping configuration and can therefore be completely neglected. Then one ends up with the well-known translational motion of hard spheres where Brownian dynamics results for the long-time diffusion coefficient are known for different packing fractions in the fluid phase [28,29]. We have systematically investigated the nontrivial cases $p=2$, 4, 6 scanning the whole density regime in the fluid phase. The shape of the rods is illustrated in Fig. 1 for these different values of p. We have taken $N=500$ rods for $p=2$, $N=540$ for $p=4$, and $N=972$ for $p=6$. Taking finite size effects properly into account, the number of rods in the cubic box has to increase with p. During the simulation the center-of-mass coordinate of the whole system was fixed in order to avoid spurious diffusion of the whole system. After each elementary trial step the orientation vectors are rescaled to have unit norm.

TABLE I. Parameters of the different runs. Given are the rod packing fraction η, the length to width ratio p, the time step Δt, the total time T over which statistics was taken, the maximal time t_m of the time window where dynamical correlations were explored, and the translational and rotational long-time self-diffusion coefficients D_L^t/D^t and D_L^r/D^r. The time unit is $\tau=\sigma^2/D_0$. The number in parentheses gives the error of the last digit.

η	p	$\Delta t/\tau$	T/τ	t_m/τ	D_L^t/D^t	D_L^r/D^r
0.1	2	0.0002	100	35	0.78(1)	0.96(1)
0.2	2	0.0002	100	35	0.607(9)	0.93(1)
0.3	2	0.0002	60	25	0.42(1)	0.84(2)
0.4	2	0.0001	60	20	0.27(1)	0.63(2)
0.5	2	0.0001	60	20	0.120(5)	0.39(1)
η_f	2	0.0001	50	20	0.035(5)	0.13(2)
0.1	4	0.0002	120	16	0.745(9)	0.82(2)
0.2	4	0.0002	60	16	0.545(9)	0.64(4)
0.3	4	0.0002	80	16	0.36(1)	0.48(2)
0.4	4	0.0002	60	16	0.215(9)	0.275(9)
η_f	4	0.0001	40	16	0.080(9)	0.10(2)
0.1	6	0.0004	35	10	0.68(1)	0.70(2)
0.2	6	0.0004	25	10	0.45(1)	0.50(2)
0.3	6	0.0002	18	8	0.31(1)	0.30(2)
η_f	6	0.0002	15	8	0.17(1)	0.13(2)
η_f	10	0.001	150	50	0.31(1)	0.19(2)
η_f	20	0.002	150	80	0.33(1)	0.11(2)

The starting configuration consisted of equally oriented square lattices which were put with different orientations on cubic sublattices of the cubic simulational box. Then with a large time step a long equilibration period was guaranteed which was checked by monitoring the mean orientation and fluctuations of the orientation as well as the mean-square displacement. Then long runs with a small time step were performed. Details and results of the different runs are listed in Table I where the time step is given in units of $\tau=\sigma^2/D_0$.

IV. ROD PAIR STRUCTURE

During the Brownian dynamics we have also calculated static averages which do not depend on the magnitude of the time step Δt. First we have computed the pair correlation function of the center of mass

$$g(r)=\frac{1}{\rho N}\sum_{i,j=1;i\neq j}^{N}\langle\delta(\mathbf{r}-(\mathbf{R}_i-\mathbf{R}_j))\rangle\ , \tag{12}$$

where $\langle\ \rangle$ denotes a canonical average. Results for $g(r)$ for different p and η are summarized in Fig. 3. For $p=2$ also $g(r)$ for hard spheres is shown exhibiting a first maximum at contact $r=\sigma$. For low packing fraction $\eta=0.2$ [Fig. 3(a)] the pair correlation exhibits an ordinary structure with a main peak between σ and the mean rod distance. For increasing p, this peak becomes broader and its amplitude decreases. In Fig. 3(b), the packing fraction is taken to be at the fluid-crystalline (fluid-nematic) coexistence line. The corresponding parameters are summarized in Table II. In these dense fluid systems, $g(r)$ shows a rich structure. For $p=2$, there is a split first maximum which can be understood as being composed by the "sphere maximum" at contact and a "configurational" maximum at mean distance

Orientational pair correlations are conveniently measured by the function [45]

$$g_P(r)=\frac{1}{\rho N g(r)}\times\sum_{i,j=1;i\neq j}^{N}\langle P_2(\cos\theta_{ij})\delta(\mathbf{r}-(\mathbf{R}_i-\mathbf{R}_j))\rangle\ , \tag{13}$$

where θ_{ij} is the angle between two orientations $\mathbf{\Omega}_i$ and $\mathbf{\Omega}_j$ and $P_2(x)=(3x^2-1)/2$ is the second Legendre polynomial. If $g_P(r)$ is positive, two rods at a given center-of-mass distance r are on average oriented in parallel whereas they are perpendicular if $g_P(r)$ has a negative sign (Fig. 4). For spherocylinders, $g_P(r)$ is positive at minimal distance. This can be understood simply by the argument that there are more configurations of vicinal cylinders with parallel orientation than that with perpendicular orientation. Due to packing effects, $g_P(r)$ has an oscillatory behavior as a function of r.

The positive sign of $g_P(r)$ near constant is in contrast to segment models with soft interactions. Due to purely energetic reasons rods are perpendicular if they are very close to each other [45,21]. This might be a mechanism to stabilize a cholesteric phase which was never found for excluded-volume interactions.

The behavior of $g(r)$ and $g_P(r)$ is not new but already

TABLE II. Packing fraction η_f of the fluid phase in coexistence with a crystalline or nematic phase for different length to width ratios p, from Refs. [59,60,22,23].

p	η_f	Coexisting phase
1	0.494	crystal
2	0.572	crystal
4	0.497	crystal
6	0.396	nematic
10	0.270	nematic
20	0.148	nematic

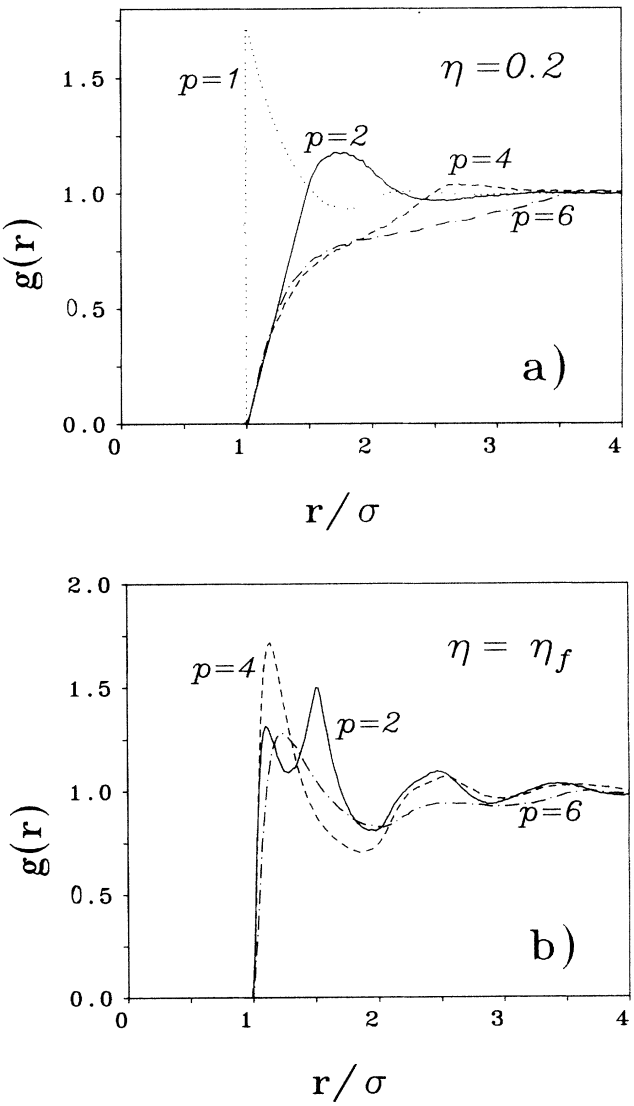

FIG. 3. Pair correlation function $g(r)$ of the center-of-mass coordinates as a function of the center-of-mass distance r measured in units of the rod diameter σ. (a) For $\eta=0.2$ and four different values of p: $p=1$ (dotted line), $p=2$ (solid line), $p=4$ (dashed line), and $p=6$ (dot-dashed line). (b) Same as (a) but now for a packing fraction corresponding to the fluid freezing line ($p=2,4$) and at the fluid-nematic transition ($p=6$). The line types are as in (a). The case $p=1$ is not shown.

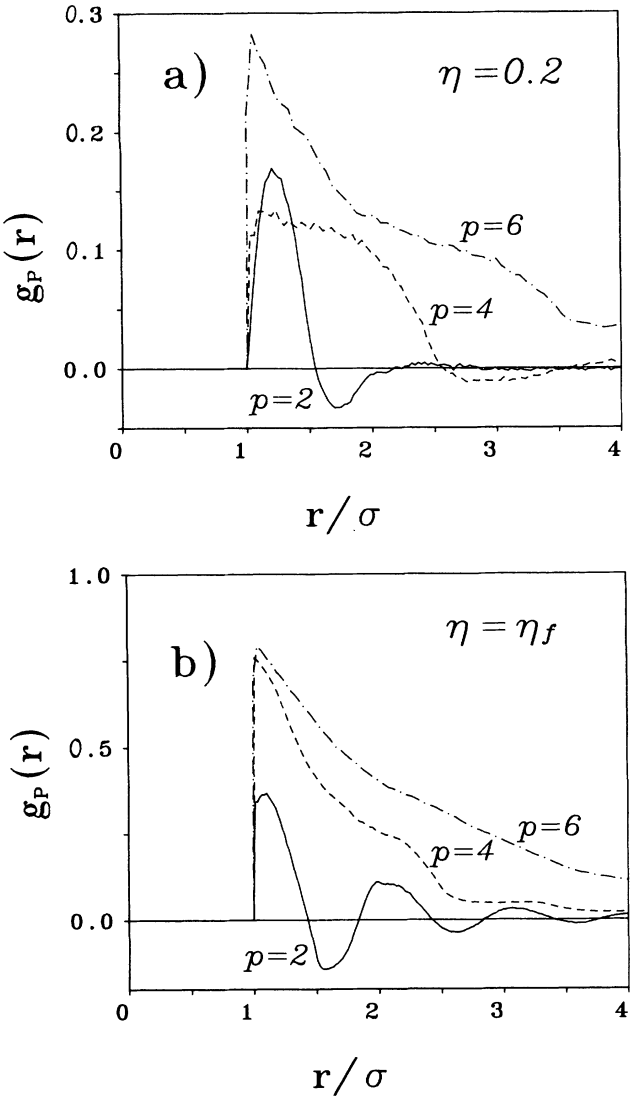

FIG. 4. Same as Fig. 3, but now for the orientational correlation function $g_P(r)$ as defined in the text. The parameters η and p and the line types are as in Figs. 3(a) and 3(b). For $p=1$, $g_P(r)$ vanishes.

known from Monte Carlo simulations [44] and integral equation theory [46]. Nonetheless we have recapitulated the basic features in order to have a feeling which structural ordering corresponds to the dynamical properties discussed in the next section.

V. TRANSLATIONAL AND ROTATIONAL LONG TIME SELF-DIFFUSION

According to Einstein's formula, the translational long-time self-diffusion coefficient D_L^t is defined as

$$D_L^t = \lim_{t\to\infty} D^t(t) \tag{14}$$

with

$$D^t(t) = W(t)/6t \ , \tag{15}$$

where

$$W(t) = \frac{1}{N}\sum_{i=1}^{N} \langle [\mathbf{R}_i(t)-\mathbf{R}_i(0)]^2 \rangle \equiv \langle [\mathbf{R}_1(t)-\mathbf{R}_1(0)]^2 \rangle \tag{16}$$

is the mean-square displacement of the center-of-mass coordinate. For large times t, the convergence of $D^t(t)$ towards D_L^t is of order $1/t$, i.e., it is rather slow. Alternatively one can define D_L^t as

$$D_L^t = \lim_{t\to\infty} \tilde{D}^t(t) \tag{17}$$

with

$$\tilde{D}^t(t) = \tfrac{1}{6}\frac{d}{dt} W(t) \ . \tag{18}$$

The latter formula has the advantage of quicker convergence as $t\to\infty$ although the statistical error is larger since it is a differential quantity. A natural scale for D_L^t is its short-time limit $D^t = \lim_{t\to 0} D^t(t)$ given by

$$D^t = \tfrac{1}{3}(2D^{\perp} + D^{\parallel}) \ . \tag{19}$$

The long-time orientational self-diffusion coefficient D_L^r, on the other hand, is defined via the long-time limit of a diffusive process on the unit sphere:

$$D_L^r = \lim_{t\to\infty} D^r(t) \tag{20}$$

with

$$D^r(t) = -\frac{1}{2t} \ln[\langle \boldsymbol{\Omega}_1(0)\cdot\boldsymbol{\Omega}_1(t)\rangle] \ . \tag{21}$$

The associated differential quantity is

$$\tilde{D}^r(t) = \frac{d}{dt}[tD^r(t)] \tag{22}$$

such that

$$D_L^r = \lim_{t\to\infty} \tilde{D}^r(t) \ . \tag{23}$$

An alternative definition for D_L^r is

$$D_L^r = -\lim_{t\to\infty} \frac{1}{6t} \ln[\langle P_2(\boldsymbol{\Omega}_1(0)\cdot\boldsymbol{\Omega}_1(t))\rangle] \ , \tag{24}$$

which has also a differential counterpart. Of course, the short-time limit $D^r = \lim_{t\to 0} D^r(t)$ provides a natural scale for $D^r(t)$.

In calculating the long-time diffusion coefficients one has two practical problems: First one has to extrapolate to infinite times, and second, as explained in Sec. III, the time step Δt has to be reasonably small. The extrapolation to infinite time is achieved by comparing $D^t(t)$ with $\tilde{D}^t(t)$. If they coincide one is very close to the infinite-time value. For the rotational diffusion, we have calculated $D^t(t), \tilde{D}^t(t)$ as well as averages of $P_2(\boldsymbol{\Omega}_i(0)\cdot\boldsymbol{\Omega}_1(t))$ as suggested by Eq. (24). In general, one needs many more configurations to get a small statistical error in the rotational relaxation than in the translational one. As regards the second difficulty, we have used a very small time step and additionally employed a simple scaling idea which is described in Appendix B to correct for finite-

time-step errors.

A typical result for time-dependent diffusion is shown in Fig. 5 where one can see that $D^t(t) \geq \tilde{D}^t(t)$ and $D^r(t) \geq \tilde{D}^r(t)$ and that the convergence of $D^t(t)$ and $D^r(t)$ is slower than that of $\tilde{D}^t(t)$ and $\tilde{D}^r(t)$. Due to the statistical noise for large times, it is very difficult to extract the leading long-time tail correction to the data. Therefore we simply focus on the long-time limit itself.

Results for the long-time self-diffusion coefficients are summarized in Table I and graphically displayed in Fig. 6 for different p as a function of η. All runs are in the fluid (disordered) phase and the whole range of packing fractions is investigated. As expected the diffusion coefficients are decreasing with increasing η. Also, for constant packing fraction, both D_L^t/D^t and D_L^r/D^r are decreasing with increasing p since there are more entangling vicinal rods for higher p. For fixed p, the data of D_L^t/D^t almost fall on a straight line. The same holds for D_L^r/D^r if p is high enough, $p \geq 4$. We have fitted the data by a simple fit formula providing an analytical expression for the long-time self-diffusion coefficients for variable p and η. A successful multiparameter fit was obtained using a polynomial expression in η and $\tilde{p} = p - 1$:

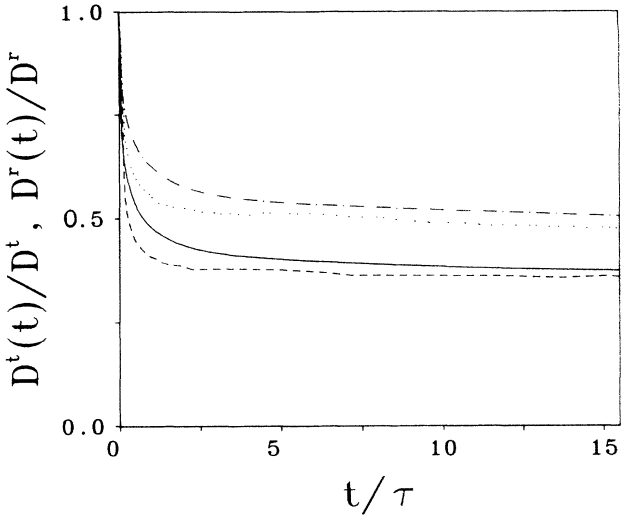

FIG. 5. Time-dependent translational and rotational diffusion coefficients $D^t(t)$ (solid line), $\tilde{D}^t(t)$ (dashed line), $D^r(t)$ (dashed-dotted line), and $\tilde{D}^r(t)$ (dotted line), as defined in the text, measured in terms of their short-time limits, $D^t = D^{\parallel} + 2D^{\perp}$ and D^r, versus t/τ. The parameters are $\eta = 0.3$ and $p = 4$.

$$D_L^t/D^t = 1 - (a_1 + a_2\tilde{p} + a_3\tilde{p}^2 + a_4\tilde{p}^3)\eta + (a_5 + a_6\tilde{p} + a_7\tilde{p}^2 + a_8\tilde{p}^3)\eta^2 + (a_9 + a_{10}\tilde{p} + a_{11}\tilde{p}^2 + a_{12}\tilde{p}^3)\eta^3 \quad (25)$$

and

$$D_L^r/D^r = 1 - (b_1\tilde{p} + b_2\tilde{p}^2 + b_3\tilde{p}^3)\eta + (b_4\tilde{p} + b_5\tilde{p}^2 + b_6\tilde{p}^3)\eta^2 + (b_7\tilde{p} + b_8\tilde{p}^2 + b_9\tilde{p}^3)\eta^3 , \quad (26)$$

where the constants are given by $a_1 = 1.940$, $a_2 = 0.310$, $a_3 = -0.0569$, $a_4 = 0.0151$, $a_5 = 1.250$, $a_6 = -0.522$, $a_7 = 0.271$, $a_8 = 0.0193$, $a_9 = -2.042$, $a_{10} = 2.836$, $a_{11} = -1.044$, $a_{12} = 0.049$, and $b_1 = 0.000$, $b_2 = 0.2897$, $b_3 = -0.0303$, $b_4 = 0.501$, $b_5 = -0.563$, $b_6 = 0.1396$, $b_7 = -7.815$, $b_8 = 4.436$, $b_9 = -0.6293$. The analytical formula is also given in Fig. 6 proving that the simple fit formula is a reasonable description for the data in the range $1 \leq p \leq 6$. We have that the analytical formula will facilitate a comparison of experimental data with the hard-spherocylinder model. It should also be useful to test theories for D_L^t/D^t and D_L^r/D^r.

One may compare our data with the theoretical expressions derived for high densities $\rho L^3 \gtrsim 100$ within the tube model of Doi and Edwards [1]

$$D_L^r/D^r = b(\rho L^3)^{-2} \quad (27)$$

and that proposed by Teraoka and Hayakawa [15]

$$D_L^r/D^r = 1/(1 + c\rho L^3)^2 , \quad (28)$$

where b and c are constants. Our data do not fulfill these relations. The reason is that ρL^3 is a small number even at freezing; our largest value for ρL^3 is 19.2 for $p = 6$ and $\eta = \eta_f$. Similar deviations from these relations for small densities were found experimentally for a charged suspension [7].

It is also interesting to check how D_L^t/D^t and D_L^r/D^r depend on the ratio of the short-time diffusion constants D^t/D^r. For spheres ($p = 1$) there is a trivial decoupling of rotation and translation, but for rods this is *a priori* not clear. We have performed runs with $D^t/D^r = 0$ as well as $D^t/D^r \to \infty$. This means that we started from an equilibrated configuration and then blocked the translational or rotational motion completely. As a result, the ratio of translational and rotational self-diffusion coefficients, obtained from a simulation where one part of motion was frozen in is significantly smaller than that from a run where both degrees of freedom were moved. Explicitly, for frozen-in motion, we found $D_L^t/D^t = 0.43$ and $D_L^r/D^r = 29$ for $p = 4$ and $\eta = 0.2$ as well as $D_L^t/D^t = 0.05$ and $D_L^r/D^r = 0.02$ for $p = 4$ and $\eta = 0.4$. This indicates a substantial coupling between translational and rotational long-time diffusion.

VI. TEST OF DYNAMICAL PHASE TRANSITION RULES FOR LIQUID CRYSTALS

For spherical interactions, empirical freezing and melting rules have proved to be very helpful in estimating fluid-solid coexistence lines. The most famous melting criterion was put forward as early as 1910 by Lindemann [47]: As an empirical fact, the ratio of the root-mean-square displacement and the average interparticle distance at the solid melting line has a value of roughly 0.15. Another freezing criterion was formulated in 1969 by Hansen and Verlet [48]. It states that the amplitude of

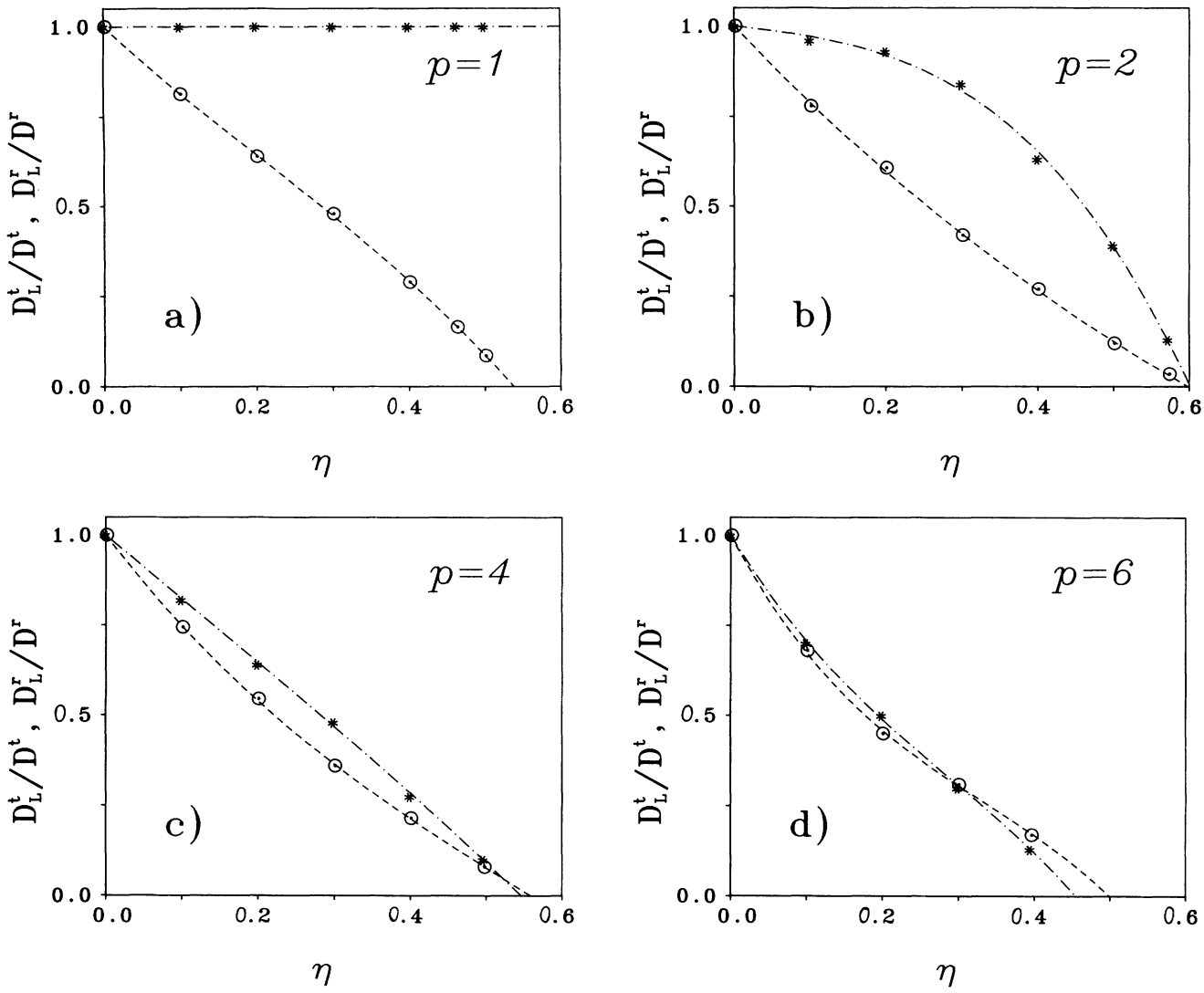

FIG. 6. Translational and rotational long-time diffusion coefficients, D_L^t (circles) and D_L^r (stars), measured in terms of their short-time limits, $D^t = D^{\parallel} + 2D^{\perp}$ and D^r, versus rod packing fraction η over the whole density regime where the fluid phase is stable. (a) For $p=1$ (spheres). From Ref. [29]. (b) For $p=2$. (c) For $p=4$. (d) For $p=6$. The lines are the analytical expressions of the fit formulas (25) and (26).

the first maximum of the liquid structure factor has a universal value of $\simeq 2.85$ along the liquid freezing line. A third *dynamical* criterion for freezing in colloidal suspensions was recently proposed by Löwen, Palberg, and Simon [31]. They found that the ratio of translational long-time and short-time self-diffusion coefficient has, within the Brownian dynamics picture, a universal value of $D_L^t/D^t = 0.098$ along the fluid freezing line. The two latter criteria are universal in the sense that they do not depend on the detailed nature of the spherical interaction potential.

For nonspherical interactions, such simple criteria are missing. For instance, the nematic orientational order parameter varies along the liquid-nematic coexistence line from 0.64 ($p=4$) to 0.80 ($p \to \infty$) [23,24]. It is tempting to check whether there are dynamical phase transition rules by looking at the values of D_L^t/D^t and D_L^r/D^r at the freezing line of the liquid. It is the advantage of our spherocylinder model that the location of this line is known: for $p=1,2,4,6$, i.e., the values investigated in this paper, there exist Monte Carlo data [22], and for $p>6$ the theory of Lee [23] gives explicit data for the coexisting fluid and nematic densities including the limit $p \to \infty$ which is known exactly from Onsager's theory [40,49,50]. Some of these freezing data are summarized in Table II. The Monte Carlo simulations have also revealed that the coexisting phase is crystalline for $p \lesssim 4.5$ whereas it is nematic for $p \gtrsim 4.5$.

In addition to the previous runs we have also performed simulations for higher p on the fluid side of the isotropic-nematic transition with $N=600$ rods for $p=10$ and $N=300$, 2400 rods for $p=20$. The results are included in Table I. For very high p ($p>30$) Onsager's theory yields an asymptotically exact expression for the fluid

density η_f at the fluid-nematic transition [49,50]:

$$\eta_f = 3.2906/p \ . \tag{29}$$

Furthermore the tube model yields $D_L^r/D^r = b(\rho L^3)^{-2}$ where an estimate of b can be obtained by fitting the simulation data of Doi, Yanamoto, and Kano resulting in $b = 540$ [9]. This yields the asymptotic prediction

$$D_L^r/D^r = 30.8/p^2 \tag{30}$$

along the fluid-nematic transition line which becomes valid for $p \gtrsim 30$. On the other hand, the translational diffusion tends to $D_L^t/D^t = 1/3$ as $p \to \infty$ according to the tube model.

In Fig. 7, D_L^t/D^t and D_L^r/D^r are plotted versus $1/p$ for η being on the fluid-freezing line. Both simulational data and the asymptotic formula (30) are shown. It turns out that along the freezing line both D_L^t/D^t and D_L^r/D^r are *nonmonotonic* with p. The translational diffusion is nonmonotonic in the crystalline region. This is connected to the nonmonotonicity in p of the coexisting fluid packing fraction η_f; see Table II. In the nematic region, D_L^t/D^t increases monotonically to its "tube limit" $\frac{1}{3}$. This limit is practically reached for $p \gtrsim 10$.

On the other hand, D_L^r/D^r is strongly decreasing for small increasing p in the crystalline region. Then, for $2 \le p \le 6$, it stays more or less constant ≈ 0.12 irrespective of whether the coexisting phase is crystalline or nematic. If p is increased further, D_L^r/D^r increases again and then decreases approaching its asymptotic law (30) for $p \gtrsim 20$.

Hence it becomes clear that both diffusion ratios D_L^t/D^t and D_L^r/D^r vary significantly along the freezing line, both in the crystalline and nematic region. Consequently a simple universal dynamical phase transition criterion which would guarantee a universal value of D_L^t/D^t or D_L^r/D^r for arbitrary p is missing. It may still be that for a fixed length to width ratio p, D_L^t/D^t and D_L^r/D^r are universal with respect to different interactions, e.g., soft Yukawa or Lennard-Jones segment forces [51]. Since for these systems the bulk phase diagram is not completely known, however, one cannot test this conjecture.

Nevertheless, in the relatively broad region $2 \le p \le 6$ where the coexisting phase may by crystalline or nematic, D_L^r/D^r is roughly constant. This is the rotational analog of the dynamical freezing rule for spherical systems: It states that an anisotropic fluid freezes if its long-time rotational self-diffusion coefficient is one order of magnitude smaller than its short-time limit. We again emphasize that this freezing rule is only valid for the restricted regime $2 \le p \le 6$.

Also the asymptotic expression (30) for D_L^r/D^r along the liquid-nematic coexistence line is useful in order to extract information on the *static* interaction from a *dynamical* measurement. There are experiments on aqueous *fd* virus solutions [7,52] measuring directly D_L^r/D^r at the fluid-nematic transition. By translating these data into our diagram one gains an effective ratio p and by the coexistence conditions an effective packing fraction which corresponds to the measured D_L^r/D^r. Thus by exploiting dynamical data one may obtain parameters of the rod interactions which are not directly accessible to static or dynamical scattering experiments. Kramer and co-workers [7,52] have measured the rotational diffusion constant for aqueous *fd* virus solutions. For their experimental parameters they found at the liquid-nematic coexistence line $D_L^r/D^r \simeq 0.05$ which correspond to an effective p of 25 with an effective packing fraction of $\eta_f = 0.13$.

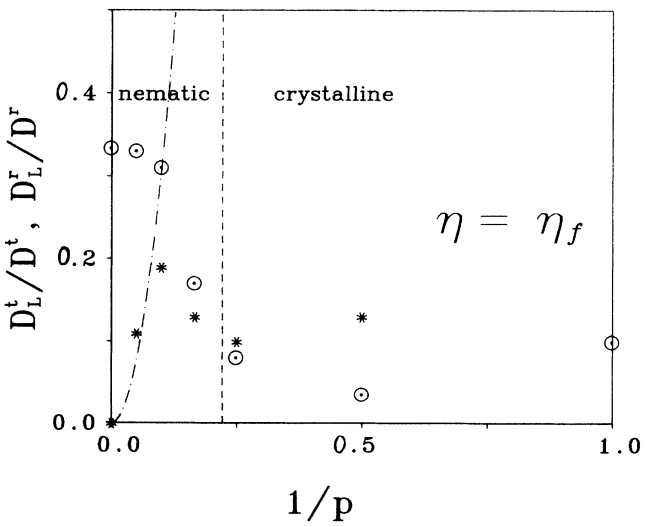

FIG. 7. Translational and rotational long-time diffusion coefficients D_L^t (circles) and D_L^r (stars), measured in terms of their short-time limits D^t and D^r, versus $1/p$ at coexistence of the liquid with the crystalline or nematic phase. The dot-dashed line is the asymptotic law (30). The dashed line separates the nematic and crystalline region.

VII. CONCLUSIONS

By computer simulation we have calculated the rotational and translational long-time self-diffusion coefficients in a fluid of hard spherocylinders exhibiting Brownian dynamics in a solvent. We end with a couple of comments related to future problems and experiments.

(i) It would be interesting to calculate the low-density correction to D_L^t/D^t and D_L^r/D^r exactly. For spheres this can be done [53,54] resulting in $D_L^t/D^t = 1 - 2\eta$ but the low density expansion is unknown for rods. Also microscopic mode-coupling theories should be extended from the spherical to the anisotropic case.

(ii) One should also examine soft interaction models (e.g., a Yukawa segment model) by Brownian dynamics simulations in order to check the influence of the finite range of the interaction potential on long-time diffusion. Work along these lines is in progress where also the dynamical scattering function is investigated and compared to experiments [55].

(iii) It has been suggested (see, e.g., [56]) that a precursor of the isotopic-nematic phase transition may be the building of so called swarms which are large nematic regions in the globally disordered fluid phase. This could slow down dramatically the rotational diffusion constant.

Since we have simulated a finite system with maximal $N=2400$ rods, we cannot test the assumption of swarms by simulation.

(iv) In order to compare with experiments one should also take the intrinsic polydispersity of the rod shape into account. One step in this direction was done by Stroobants [57], who recently simulated the phase diagram of a bidisperse rod system with fixed orientation.

ACKNOWLEDGMENTS

I thank G. Szamel, H. Spohn, T. Kirchhoff, R. Klein, T. Palberg, and J.-L. Barrat for helpful discussions. This work was supported by the Bundesministerium für Forschung und Technologie (BMFT) under Contract No. 03-WA3LMU.

APPENDIX A: CONDITIONS FOR ROD OVERLAP

Two spherocylinders with center-of-mass coordinates $\mathbf{R}_1,\mathbf{R}_2$ and orientations $\mathbf{\Omega}_1,\mathbf{\Omega}_2$ are overlapping if at least one of the nine following conditions is satisfied.

(1) Mutual penetration of the cylindric parts:

$$\left|\frac{\mathbf{r}\cdot\mathbf{\Omega}_2-(\mathbf{\Omega}_1\cdot\mathbf{\Omega}_2)(\mathbf{r}\cdot\mathbf{\Omega}_1)}{1-(\mathbf{\Omega}_1\cdot\mathbf{\Omega}_2)^2}\right|\leq(L-\sigma)/2 \tag{A1}$$

and

$$\left|\frac{\mathbf{r}\cdot\mathbf{\Omega}_1-(\mathbf{\Omega}_1\cdot\mathbf{\Omega}_2)(\mathbf{r}\cdot\mathbf{\Omega}_2)}{1-(\mathbf{\Omega}_1\cdot\mathbf{\Omega}_2)^2}\right|\leq(L-\sigma)/2 \tag{A2}$$

and

$$\left|\mathbf{r}\cdot\frac{(\mathbf{\Omega}_1\times\mathbf{\Omega}_2)}{|\mathbf{\Omega}_1\times\mathbf{\Omega}_2|}\right|\leq\sigma\ , \tag{A3}$$

where $\mathbf{r}=\mathbf{R}_2-\mathbf{R}_1$.

(2)–(5) There are four possibilities for overlapping spheres being at the top and bottom of the spherocylinders which are captured by the four conditions

$$|\mathbf{x}-\mathbf{y}|\leq\sigma\ , \tag{A4}$$

with $\mathbf{x}=\mathbf{R}_1\pm(L-\sigma)\mathbf{\Omega}_1/2$ and $\mathbf{y}=\mathbf{R}_2\pm(L-\sigma)\mathbf{\Omega}_2/2$.

(6) and (7) Penetration of a sphere of the first rod with the cylindric part of the second rod. There are two double conditions:

$$|\mathbf{x}\cdot\mathbf{\Omega}_2|\leq(L-\sigma)/2 \tag{A5}$$

and

$$|\mathbf{x}-(\mathbf{x}\cdot\mathbf{\Omega}_2)\mathbf{\Omega}_2|\leq\sigma \tag{A6}$$

with $\mathbf{x}=\mathbf{R}_1\pm(L-\sigma)\mathbf{\Omega}_1/2$.

(8) and (9) Penetration of a sphere of the second rod with the cylindric part of the first rod. Again there are two double conditions:

$$|\mathbf{y}\cdot\mathbf{\Omega}_1|\leq(L-\sigma)/2 \tag{A7}$$

and

$$|\mathbf{y}-(\mathbf{y}\cdot\mathbf{\Omega}_1)\mathbf{\Omega}_1|\leq\sigma \tag{A8}$$

with $\mathbf{y}=\mathbf{R}_2\pm(L-\sigma)\mathbf{\Omega}_2/2$.

APPENDIX B: FINITE TIME-STEP CORRECTIONS VIA A SCALING METHOD

Since long-time self-diffusion data of hard bodies depend sensitively on the time step used in the Brownian dynamics simulation, one has in principle to perform a run with different time steps and extrapolate the diffusion data to a time step of zero. The problem is how to do this extrapolation explicitly. For spheres two different schemes were proposed by Cichocki and Hinsen [28,29] leading to slightly different results for the long-time self-diffusion coefficient. A simpler version where overlapping spheres are shifted until they touch was successfully implemented by Schaertl and Sillescu [58]. The latter method is very efficient, but fails for high packing fractions. Unfortunately both methods cannot be directly transferred to rods.

In this appendix, a simple scaling correction is proposed to avoid errors due to a finite time step. The method is most easily explained for the isotropic case of spheres. If a finite time step Δt is used, two spheres will have a large probability to overlap after the next time step if they have a distance of $\sigma_{\text{eff}}=\sigma+\Delta R$. Here

$$\Delta R=\sqrt{6D_s\Delta t}\ , \tag{B1}$$

where D_s is the isotropic short-time diffusion constant of hard spheres. As far as dynamical long-time properties are concerned, the idea is that the spheres behave effectively as a system with a larger diameter σ_{eff} instead of their bare diameter σ. The system simulated with a finite time step thus effectively has a larger packing fraction which reduces the long-time diffusion coefficient. By examining the finite time-step analysis of Ref. [28] where a packing fraction of $\eta=0.4$ was taken, it turns out that the reduced long-time diffusion coefficient can be perfectly understood quantitatively as belonging to a larger packing fraction determined by the larger diameter σ_{eff}. Inversely, for a given packing fraction and a finite time step, one should thus simulate a system with a smaller packing fraction in order to get the correct long-time behavior.

This scaling concept has the advantage of being easily transferable to rodlike particles. In this case one has an averaged parallel displacement $x^{\parallel}=\sqrt{2D^{\parallel}\Delta t}$, a perpendicular translational displacement $x_1^{\perp}=\sqrt{2D^{\perp}\Delta t}$, and a perpendicular rotational displacement $x_2^{\perp}=\sqrt{2D^{r}\Delta t}\,L/2$ for a point on the top of the spherocylinder. For a given bare cylinder diameter σ and total length L we consider an effective spherocylinder with smaller diameter σ' and different total length L' in order to eliminate corrections due to the finite time step. Explicitly we take

$$\sigma'=\sigma-\sqrt{2}x_1^{\perp}-\tfrac{1}{2}x_2^{\perp} \tag{B2}$$

and

$$L'=L-x^{\parallel}+(\sigma'-\sigma)\ . \tag{B3}$$

For $p=2$ we have systematically examined the effect of this scaling. The translational and rotational long-time self-diffusion coefficients of the scaled spherocylinders agree quite well with that of the original system, simulated with a much smaller time step. For all parameter combinations, we have used both the original and the scaled system with the same time step. The differences in long-time diffusion are on the 5% level. This finally provides an efficient way to estimate errors due to a finite time step.

[1] M. Doi and S. F. Edwards, *The Theory of Polymer Dynamics* (Oxford University Press, Oxford, 1986).

[2] J. F. Maguire, J. P. McTague, and F. Rondelez, Phys. Rev. Lett. **45**, 1891 (1980).

[3] H. Nakamura and K. Okano, Phys. Rev. Lett. **50**, 186 (1983).

[4] S. F. Schulz, E. E. Maier, R. Krause, M. Hagenbüchle, M. Deggelmann, and R. Weber, J. Chem. Phys. **92**, 7087 (1990).

[5] M. Hagenbüchle, C. Graf, and R. Weber, Prog. Colloid Polym. Sci. **89**, 49 (1992).

[6] C. Graf, M. Deggelmann, M. Hagenbüchle, H. Kramer, R. Krause, C. Martin, and R. Weber, J. Chem. Phys. **95**, 6284 (1991).

[7] H. Kramer, M. Deggelmann, C. Graf, M. Hagenbüchle, C. Johner, and R. Weber, Macromolecules **25**, 4325 (1992).

[8] R. Simon, T. Palberg, and P. Leiderer, J. Chem. Phys. **99**, 3030 (1993).

[9] M. Doi, I. Yanamoto, and F. Kano, J. Phys. Soc. Jpn. **53**, 3000 (1984).

[10] M. Fixman, Phys. Rev. Lett. **54**, 337 (1985); **55**, 2429 (1985).

[11] I. Bitsanis, H. T. Davis, and M. Tirrell, Macromolecules **21**, 2824 (1988); **23**, 1157 (1990).

[12] M. Doi, J. Phys. (Paris) **36**, 607 (1975).

[13] M. Doi and S. F. Edwards, J. Chem. Soc. Faraday Trans. **74**, 560 (1978); **74**, 918 (1978).

[14] I. Teraoka, N. Ookubo, and R. Hayakawa, Phys. Rev. Lett. **55**, 2712 (1985).

[15] I. Teraoka and R. Hayakawa, J. Chem. Phys. **91**, 2643 (1989).

[16] G. Szamel, Phys. Rev. Lett. **70**, 3744 (1993).

[17] C. F. Wu, S. H. Chen. L. B. Shih, and J. S. Lin, Phys. Rev. Lett. **61**, 645 (1988).

[18] J. Schneider, W. Hess, and R. Klein, J. Phys. A **18**, 1221 (1985).

[19] J. Schneider, W. Hess, and R. Klein, Macromolecules **19**, 1729 (1986).

[20] J. Schneider, D. Karrer, J. K. G. Dhont, and R. Klein, J. Chem. Phys. **87**, 3008 (1987).

[21] H. Löwen, Phys. Rev. Lett. **72**, 424 (1994).

[22] J. A. C. Veerman and D. Frenkel, Phys. Rev. A **41**, 3237 (1990). Note that in this reference L does not denote the total rod length but that of the cylindric part.

[23] S.-D. Lee, J. Chem. Phys. **87**, 4972 (1987).

[24] A. Poniewierski and R. Holyst, Phys. Rev. Lett. **61**, 2461 (1988); Phys. Rev. A **41**, 6871 (1990).

[25] D. W. Rebertus and K. M. Sando, J. Chem. Phys. **67**, 2585 (1977).

[26] D. Frenkel and J. F. Maguire, Phys. Rev. Lett. **47**, 1025 (1981).

[27] P. Bereolos, J. Talbot, M. P. Allen, and G. T. Evans, J. Chem. Phys. **99**, 6087 (1993).

[28] B. Cichocki and K. Hinsen, Physica A **166**, 473 (1990).

[29] B. Cichocki and K. Hinsen, Physica A **187**, 133 (1992).

[30] J. A. Leegwater and G. Szamel, Phys. Rev. A **46**, 4999 (1992); **46**, 5012 (1992).

[31] H. Löwen, T. Palberg, and R. Simon, Phys. Rev. Lett. **70**, 1557 (1993).

[32] H. Löwen and G. Szamel, J. Phys. Condens. Matter **5**, 2295 (1993).

[33] F. Bitzer, T. Palberg, H. Löwen, R. Simon, and P. Leiderer, Phys. Rev. E (to be published).

[34] N. J. Wagner, R. Krause, A. R. Rennie, B. D'Aguanno, and J. Goodwin, J. Chem. Phys. **95**, 494 (1991).

[35] G. Nägele, T. Zwick, R. Krause, and R. Klein, J. Colloid Interface Sci. **161**, 347 (1993).

[36] S. Broersma, J. Chem. Phys. **32**, 1626 (1960); **32**, 1632 (1960); **74**, 6989 (1981).

[37] M. M. Tirado and J. G. de la Torre, J. Chem. Phys. **71**, 2581 (1979); **73**, 1986 (1980).

[38] M. M. Tirado, C. L. Martinez, and J. G. de la Torre, J. Chem. Phys. **81**, 2047 (1984).

[39] S. Fraden, G. Maret, D. L. D. Caspar, and R. B. Meyer, Phys. Rev. Lett. **63**, 2068 (1989); X. Wen, R. B. Meyer, and D. L. D. Caspar, *ibid.* **63**, 2760 (1989).

[40] L. Onsager, Ann. N.Y. Acad. Sci. **51**, 627 (1949).

[41] M. Medina-Noyola, Phys. Rev. Lett. **60**, 2705 (1988).

[42] D. L. Ermak, J. Chem. Phys. **62**, 4189 (1975); **64**, 4197 (1975).

[43] H. Löwen, J-P. Hansen, and J. N. Roux, Phys. Rev. A **44**, 1169 (1991).

[44] I. Nezbeda, Czech. J. Phys. B **26**, 1087 (1976).

[45] R. Klein, in *Structure and Dynamics of Strongly Interacting Colloids and Supramolecular Aggregates in Solution,* Vol. 369 of *NATO Advanced Study Institute,* edited by S. H. Chen, J. S. Huang, and P. Tartaglia (Kluwer Academic, Dordrecht, 1992).

[46] A. Perera and G. N. Patey, J. Chem. Phys. **89**, 5861 (1988).

[47] F. A. Lindemann, Phys. Z. **11**, 609 (1910); see also A. R. Ubbelohde, *The Molten State of Matter* (Wiley, Chicester, 1978).

[48] J. P. Hansen and L. Verlet, Phys. Rev. **184**, 151 (1969).

[49] G. Lasher, J. Chem. Phys. **53**, 4141 (1970).

[50] R. F. Kayser and H. J. Raveche, Phys. Rev. A **17**, 2067 (1978).

[51] G. V. Paolini, G. Ciccotti, and M. Ferrario, Mol. Phys. **80**, 297 (1993).

[52] H. Kramer, Ph.D. thesis, Universität Konstanz, 1993.

[53] B. J. Ackerson and L. Fleishman, J. Chem. Phys. **76**, 2675 (1982).

[54] S. Hanna, W. Hess, and R. Klein, Physica A **111**, 181 (1982).

[55] T. Kirchhoff, H. Löwen, and R. Klein (unpublished).

[56] P. G. de Gennes, *The Physics of Liquid Crystals* (Clarendon, Oxford, 1974).

[57] A. Stroobants, Phys. Rev. Lett. **69**, 2388 (1992).

[58] W. Schaertl and H. Sillescu, J. Colloid Interface Sci. **155**, 313 (1993); J. Stat. Phys. **74**, 687 (1994).

[59] W. G. Hoover and F. H. Ree, J. Chem. Phys. **49**, 3609 (1968).

[60] D. Frenkel, H. N. W. Lekkerkerker, and A. Stroobants, Nature (London) **332**, 822 (1988).

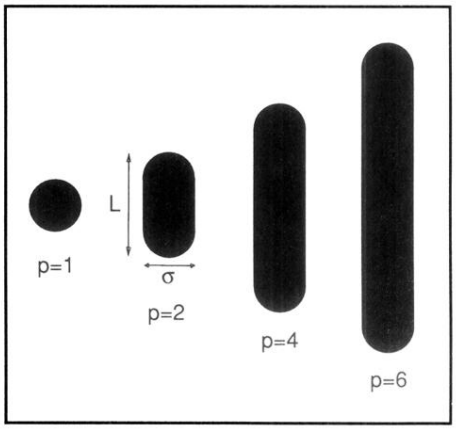

FIG. 1. Shape of the spherocylinders for different values of the length to width ratio $p = L/\sigma$. The cases $p = 1,2,4,6$ which are used in the simulations are shown.